

# Reconstruction of a persistent random walk from exit time distributions

Pak-Wing Fok<sup>1</sup>, Qunhui Han<sup>1</sup>, and Tom Chou<sup>2</sup>

<sup>1</sup>Dept. of Mathematical Sciences, University of Delaware, DE 19716

<sup>2</sup>Dept. of Biomathematics & Dept. of Mathematics, UCLA, Los Angeles, CA 90095

March 4, 2013

## Abstract

In this paper, we study the inverse problem of reconstructing the spatially dependent transition rate  $F(x)$  of a one-dimensional Broadwell process from exit time distributions. In such a process, an advecting particle is assumed to undergo transitions between states with constant positive ( $+v$ ) and negative ( $-v$ ) velocities. The goal is to reconstruct the transition rate function  $F(x)$  from the exit time distributions out of a finite interval. Using the associated backward equation, we compute the distribution of exit times and its Laplace transform, given a fixed starting position and velocity. We propose two methods (called ‘ $t$ ’ and ‘ $s$ ’) for finding  $F(x)$ . In both methods, we represent  $F(x)$  as a linear combination of polynomials and repeatedly solve the backward equation to minimize the difference between its solution and given first exit time data. In the  $t$ -method we work in the time domain, using exit times directly and leveraging a novel series solution for the exit time distribution. In the  $s$ -method, we work with the Laplace-transformed equation and Laplace-transformed exit times. Noisy data is generated using a custom-designed algorithm to simulate the trajectories of a Broadwell process. In most cases we can find 4 coefficients to within  $O(10^{-1})$  accuracy from  $O(10^4)$  exit times, with the  $t$ -method method slightly out-performing the  $s$ -method. We also explore the effectiveness of our algorithms for a fixed number of exit times under different advection speeds and find that optimal reconstruction occurs when  $v = O(1)$ .

Keywords: Random Walk, Inverse Problem, Broadwell, Telegrapher’s equation

## 1 Introduction

Inverse problems arise in many applications such as medical imaging [1], high energy particle physics [21], and seismology [9]. Most of these applications involve measurement of waves at

4 the boundary of a domain; from this boundary data one may wish to reconstruct spatially-  
5 dependent properties within the domain such as the density and/or wave speed. However,  
6 there have been fewer successful applications where the underlying physics involves an in-  
7 trinsic random process. The corresponding “boundary data” for stochastic inverse problems  
8 are probability fluxes or exit time distributions. The types of stochastic inverse problems  
9 we are concerned with in this paper involve inferring the parameters of a stochastic process  
10 from such a distribution.

11 One example of such a stochastic inverse problem arises in the reconstruction of bond  
12 potentials from rupture time distributions [10, 12, 17]. In force spectroscopy experiments, an  
13 increasing force is applied across a macromolecular bond until it ruptures. Because of thermal  
14 fluctuations, the rupture force is a random variable; thus the goal is to infer properties of  
15 the bond potential from the *distribution* of rupture forces. Stochastic inverse problems also  
16 commonly arise in diffuse optical tomography [1, 2]. In all these applications, the exit time  
17 distribution of a Brownian motion leaving a finite interval is measured, and one wishes to  
18 reconstruct the drift and/or diffusion function.

19 While Brownian motion is a canonical stochastic model, the inverse problem associated  
20 with Brownian motion is ill-posed [4, 11] and motivates the study of stochastic exit time  
21 problems based on other types of random walk. Ill-posedness is a trademark of many inverse  
22 problems. A problem is *well-posed* if a solution exists, is unique and depends continuously on  
23 the data. Otherwise the problem is *ill-posed*. At present, issues of existence and uniqueness of  
24 spatially dependent parameters for random walks are generally not well established, although  
25 some important results for Brownian motions can be found in [4].

26 In this paper, we generalize the study of Brownian inverse problems by focusing on a class  
27 of persistent random walk models called Broadwell processes [6, 7, 8, 16, 20]. In a Broadwell  
28 process, a particle randomly interconverts (“flips”) between multiple states with each state  
29 associated with a particular velocity. The Broadwell process has the desirable property that  
30 it interpolates between a ballistic and diffusive motion [5, 22]: the time between transitions  
31 decreases as the flip rate increases, but increases as the flip rate decreases. The Broadwell  
32 model opens the analysis of the inverse problem for these two types of limiting processes;  
33 studying the inverse Broadwell problem may therefore provide insight into the important,  
34 fully diffusive problem. We specialize to the constant speed Broadwell process, assuming  
35 that transition probabilities that are spatially dependent and that the particle takes only two  
36 states associated with a positive and negative velocity. From the distribution of exit times  
37 out of a finite interval, our goal is to find the transition probability (“flip-rate”) function.

38 Accurately simulating the exit times of a Brownian motion can be quite involved although  
39 reliable methods do exist: see [14, 15, 19, 25] for example. Nevertheless, one important  
40 advantage of studying the Broadwell model is the ease with which it can be simulated.  
41 Accurate simulations are critical for comparisons between reconstructed flip-rate functions  
42 and the underlying target functions that produced the exit data. When generating the exit  
43 time distribution from our simulations, the only source of error (besides round-off) stems  
44 from using a finite number of realizations.

45 The outline of this paper is as follows. In section A, we derive from first principles the  
46 Backward Kolmogorov Equation (BKE) for a general  $K$ -state Broadwell process. We then  
47 restrict our attention to the simple two-state case parameterized by a spatially dependent

48 (but state-symmetric) transition rate and a constant speed. We also state the inverse prob-  
 49 lem of reconstructing the flip-rate function from the exit time distributions. The associated  
 50 optimization problem involves minimizing the distance between the solution of the BKE and  
 51 the exit time data (derived from simulations or from the solution of the BKE with a given  
 52 flip rate function). In section 2 we discuss the numerical aspects of our work. In partic-  
 53 ular, we present two reconstruction methods. The first involves minimizing the difference  
 54 between the solution to the BKE and the target data in the time domain. The second in-  
 55 volves minimizing the difference between the Laplace-transformed solution of the BKE and  
 56 transformed exit time data. We also explain the simulation of Broadwell random walkers to  
 57 test our reconstruction protocols. In Section 3 we present the results of our reconstruction  
 58 using noisy data and compare the two methods. We show that for a finite number of exit  
 59 times, the most reliable reconstruction of the flip rate occurs at an intermediate advection  
 60 speed, no matter which method is used. In Section 4, we discuss general implications of our  
 61 results and summarize our findings.

## 62 1.1 Two-state model and statement of inverse problem

63 A two-state Broadwell model describes a particle that can take one of two states. Initially,  
 64 the particle is at position  $x$  and in state  $i \in \{1, 2\}$ . The particle advects within an interval  
 65  $(-L/2, L/2)$  with velocity  $+v$  if  $i = 1$  and  $-v$  if  $i = 2$ . While advecting, the particle may  
 66 change state with probability  $F(y)dt$  within time interval  $(t, t + dt)$  where  $y$  is the current  
 67 particle position.

68 Let  $w(t|x, 1, 0) \equiv w_1(x, t)$  and  $w(t|x, 2, 0) = w_2(x, t)$  be the exit time distributions condi-  
 69 tioned on the particle initially being at position  $x$  and having a positive ( $+v$ ) and negative  
 70 ( $-v$ ) velocity respectively. Then the exit time distributions satisfy

$$\frac{\partial w_1}{\partial t} = v \frac{\partial w_1}{\partial x} + F(x)(w_2 - w_1), \quad (1)$$

$$\frac{\partial w_2}{\partial t} = -v \frac{\partial w_2}{\partial x} + F(x)(w_1 - w_2), \quad (2)$$

71 subject to initial conditions

$$w_1(x, 0) = 0, \quad w_2(x, 0) = 0. \quad (3)$$

72 and boundary conditions

$$w_1(x = L/2, t) = \delta(t), \quad w_2(x = -L/2, t) = \delta(t). \quad (4)$$

73 A full derivation of the backward equation for the exit time distribution for a general  $K$ -state  
 74 Broadwell process (of which (1)-(4) are a special case) can be found in Appendix A.

75 Given  $F(x)$ , one can solve eqs. (1)-(3) (the “forward problem”) to find  $w_1(x, t)$  and  $w_2(x, t)$   
 76 for all  $-L/2 < x < L/2$  and  $t > 0$ . Note that eqs. (1) and (2) constitute Kolmogorov’s  
 77 backward equations for the exit time distributions, and that solving this backward equation  
 78 defines the *forward* problem for computing  $w_1(x, t)$ ,  $w_2(x, t)$  from a known  $F(x)$ . However in

79 this paper we are interested in the *inverse* problem:

80

81 **Problem Statement:** Consider eqs. (1)-(3). Given a known, fixed  $-L/2 < x_0 < L/2$ ,  
 82 a known velocity  $v > 0$  and exit time distributions  $w_1(x_0, t)$  and  $w_2(x_0, t)$  for  $t > 0$ , find  
 83  $F(x) \in C(-L/2, L/2)$ .

84

85 In practice, the exit time distributions could come from directly simulating a Broadwell  
 86 process or from a single solution of the forward problem. For particles that initially advect  
 87 with velocities  $+v$  and  $-v$ , we refer to associated exit time distributions  $w_{1,\text{data}}(x_0, t)$  and  
 88  $w_{2,\text{data}}(x_0, t)$  respectively; note that  $w_{1,\text{data}}(x_0, t)$  and  $w_{2,\text{data}}(x_0, t)$  may or may not be noisy.  
 89 We give details on how  $w_{1,\text{data}}$  and  $w_{2,\text{data}}$  are computed in Section 2.2.

90 Unfortunately, eqs. (1)-(3) are not useful in practice for inferring  $F(x)$  because the so-  
 91 lutions are highly singular. Related quantities that are more regular and whose governing  
 92 equations are more amenable to numerical methods are the cumulative density functions  
 93 (cdfs) and Laplace-transformed probability density functions. We now give explicit forms for  
 94 these equations since we make frequent use of them later on.

95 The cdfs are related to the pdfs by  $W_{1,2}(x, t) = \int_0^t w_{1,2}(x, t') dt'$ . Therefore, upon inte-  
 96 grating (1) and (2) in time, we find

$$\frac{\partial W_1}{\partial t} - v \frac{\partial W_1}{\partial x} = F(x)(W_2 - W_1), \quad (5)$$

$$\frac{\partial W_2}{\partial t} + v \frac{\partial W_2}{\partial x} = F(x)(W_1 - W_2), \quad (6)$$

97 subject to the boundary conditions

$$W_1(L/2, t) = H(t), \quad W_2(-L/2, t) = H(t), \quad (7)$$

98 and initial conditions

$$W_1(x, 0) = 0, \quad W_2(x, 0) = 0. \quad (8)$$

99 In eqs. (7),  $H(t)$  is the Heaviside step function satisfying  $H(t) = 1$  if  $t > 0$  and  $H(t) = 0$   
 100 if  $t \leq 0$ . The corresponding inverse problem is to find  $F(x) \in C(-L/2, L/2)$  given  $-L/2 <$   
 101  $x_0 < L/2$ ,  $v$  and  $W_{j,\text{data}}(x_0, t) = \int_0^t w_{j,\text{data}}(x_0, t') dt'$  for  $t > 0$  and  $j = 1, 2$ . Alternatively, we  
 102 can also take Laplace transforms of (1) and (2) to find

$$s\tilde{w}_1(x, s) = v \frac{\partial \tilde{w}_1}{\partial x} + F(x)(\tilde{w}_2 - \tilde{w}_1), \quad (9)$$

$$s\tilde{w}_2(x, s) = -v \frac{\partial \tilde{w}_2}{\partial x} + F(x)(\tilde{w}_1 - \tilde{w}_2), \quad (10)$$

103 subject to boundary conditions

$$\tilde{w}_1(x = L/2, s) = 1, \quad \tilde{w}_2(x = -L/2, s) = 1. \quad (11)$$

104 The corresponding inverse problem is to find  $F(x) \in C(-L/2, L/2)$  given  $-L/2 < x_0 < L/2$ ,  
 105  $v$  and  $\tilde{w}_{j,\text{data}}(x_0, s)$  for  $s > 0$  and  $j = 1, 2$ .

## 2 Algorithms for Reconstruction

This section is divided into 3 parts. First, we give details on solving the forward problems (9)-(11) and (5)-(8). Then we explain how to generate noisy data by directly simulating a Broadwell process with spatially dependent flip rate. Finally, we discuss a projection method to solve the inverse problem.

### 2.1 Solution to the forward problems

**Solution to (9)-(11):** Our method for finding  $\tilde{w}_1(x_0, s)$  and  $\tilde{w}_2(x_0, s)$  from eqs. (9)-(11) is based on solving the boundary value problem using a pseudospectral method [26] for different values of  $s \geq 0$ : see Algorithm 1. The solutions  $\tilde{w}_{1,2}(x_0, s)$  are always infinitely differentiable, monotonically decreasing functions in  $s$  that  $\rightarrow 0$  as  $s \rightarrow \infty$ .

---

**Algorithm 1** Algorithm for solving the forward problem (9)-(11).

---

- 1: Require: flip rate function  $F(x)$ , velocity  $v > 0$ , interval size  $L$ , starting position  $-L/2 < x_0 < L/2$  and integer  $N \gg 1$ .
  - 2: **for**  $i = 1, 2, \dots, N$  **do**
  - 3:   let  $\xi_i = (i - 1)/N$  and  $s_i = \xi_i/(1 - \xi_i)$ .
  - 4:   With  $s = s_i$ , solve (9)-(11) using a pseudospectral discretization [26] in  $x$ .
  - 5:   Interpolate the solution at  $x = x_0$  to find  $\tilde{w}_1(x_0, s_i)$  and  $\tilde{w}_2(x_0, s_i)$ .
  - 6: **end for**
  - 7: Output: Laplace Transformed exit time distributions  $\tilde{w}_1(x_0, s_i)$  and  $\tilde{w}_2(x_0, s_i)$ ,  $i = 1, \dots, N$ .
- 

**Solution to (5)-(8):** In contrast to  $\tilde{w}_{1,2}(x_0, s)$ , the solutions  $W_{1,2}(x, t)$  contain jump discontinuities that propagate into the domain of solution with velocity  $\pm v$ : the jump discontinuity in  $W_1(x, t)$  ( $W_2(x, t)$ ) propagates along the characteristic line  $t = -x/v + L/(2v)$  ( $t = +x/v + L/(2v)$ ). This behavior in the singularities is illustrated by the following theorem which uses an eigenfunction expansion to construct an explicit solution to (5)-(8).

**Theorem 1** (Series solution to the forward problem (5)-(8)). *For  $0 < t < L/v$ , the solution to (5)-(8) is*

$$W_1(x, t) = a_1(x)H[t + x/v - L/(2v)] + Z_1(x, t), \quad (12)$$

$$W_2(x, t) = a_2(x)H[t - x/v - L/(2v)] + Z_2(x, t), \quad (13)$$

where  $H[\cdot]$  is the heaviside step function and  $Z_{1,2}(x, t)$  are continuous functions given by the series

$$\mathbf{Z}(x, t) = - \sum_{m=1}^{\infty} \frac{\mathbf{u}_m(x)}{s_m D_m} [h_m^{(1)}(t) + h_m^{(2)}(t)], \quad (14)$$

126 where:

$$h_m^{(1)}(t) = \int_{-L/2}^{-L/2+vt} p_m^{(1)*}(y) a_2(y) F(y) (1 - e^{(t-\frac{y}{v}-\frac{L}{2v})s_m}) dy, \quad (15)$$

$$h_m^{(2)}(t) = \int_{L/2-vt}^{L/2} p_m^{(2)*}(y) a_1(y) F(y) (1 - e^{(t+\frac{y}{v}-\frac{L}{2v})s_m}) dy, \quad (16)$$

$$a_1(x) = \exp \left[ -\frac{1}{v} \int_x^{L/2} F(x') dx' \right], \quad (17)$$

$$a_2(x) = \exp \left[ -\frac{1}{v} \int_{-L/2}^x F(x') dx' \right], \quad (18)$$

$$D_m = \langle \mathbf{p}_m(x), \mathbf{u}_m(x) \rangle = \int_{-L/2}^{L/2} \mathbf{p}_m^*(x) \mathbf{u}_m(x) dx. \quad (19)$$

127 In (14),  $s_m \in \mathbb{C}$  and  $\mathbf{u}_m(x) \in \mathbb{C}^2$  are the eigenvalues and eigenfunctions of  $\mathbf{A}$  where

$$\mathbf{A} \begin{pmatrix} u_1 \\ u_2 \end{pmatrix} = \left\{ \begin{bmatrix} v \frac{d}{dx} & 0 \\ 0 & -v \frac{d}{dx} \end{bmatrix} + F(x) \begin{bmatrix} -1 & 1 \\ 1 & -1 \end{bmatrix} \right\} \begin{pmatrix} u_1(x) \\ u_2(x) \end{pmatrix}, \quad (20)$$

128 along with the boundary conditions  $u_1(L/2) = u_2(-L/2) = 0$ .  $\mathbf{p}_m(x) = [p_m^{(1)}(x), p_m^{(2)}(x)]^T$   
 129 are the eigenfunctions of the adjoint operator  $\mathbf{A}^*$ .

130 We now discuss the behavior of the solutions  $W_{1,2}(x, t)$  in light of eqs. (12)-(13) and  
 131 defer the proof of the theorem to the end of this section. From (12) and (13) it is clear that  
 132 discontinuities in the boundary conditions (7) propagate into the interior. In Figure 1(a),  $W_1$   
 133 is discontinuous on the diagonal line separating  $A, C$  and  $B, D$  while  $W_2$  is discontinuous on the  
 134 line separating  $A, D$  and  $B, C$ . Because the hyperbolic system (5)-(8) has a finite wave speed  
 135  $v > 0$ , region  $C$  is outside the region of influence of the disturbances originating at  $(x, t) =$   
 136  $(L/2, 0)$  and  $(-L/2, 0)$  and we expect that  $W_1(x, t) = W_2(x, t) = 0$  in  $C$ . This behavior  
 137 is confirmed in Figure 1(b) which shows the cumulative distribution functions  $W_{1,2}(x =$   
 138  $-L/4, t)$  calculated using (12)-(14). The function  $W_1(-L/4, t)$  has a discontinuous derivative  
 139 at  $t_1 = L/(4v)$  and a jump discontinuity at  $t_2 = 3L/(4v)$  while  $W_2(-L/4, t)$  has a jump  
 140 discontinuity at  $t_1$  and a discontinuous derivative at  $t_2$ . Figure 1(c) shows cdfs evaluated  
 141 at  $x_0 = L/3$ . The inset shows associated Laplace-transformed probability density functions  
 142  $\tilde{w}_1(L/3, s)$  and  $\tilde{w}_2(L/3, s)$ , found by solving eqs. (9)-(11) using Algorithm 1. Cumulative  
 143 density functions from Monte-Carlo simulations are superposed to validate our numerical  
 144 method; details of how these simulations are performed are described in section 2.2.

145 The expansions (12)-(13) in Theorem 1 are commonly used to analyze seismic waves  
 146 [9, 23, 24] and form the basis of our numerical method for the forward problem in  $t$ : see  
 147 Algorithm 2. Numerically, the cdfs  $W_{1,2}$  are computed by taking a finite number of terms  
 148 in (14) and adding on a step discontinuity at  $t = \mp x/v + L/(2v)$  with strength given by  
 149 (17) and (18). A pseudo-spectral collocation method on a Chebyshev grid was used to find  
 150 the eigenvectors  $\mathbf{u}_j$  and Clenshaw-Curtis quadrature [26] was used to quickly evaluate the

---

**Algorithm 2** Algorithm for solving the forward problem (5)-(8). The same symbol is used to refer to quantities in (14)-(19) as well as their numerical approximations. For example,  $\mathbf{A}$  refers to the differential operator as well as its matrix approximation.

---

- 1: Require: A target flip rate  $F(x)$ , velocity  $v > 0$ , an integer  $N$ , a starting position  $-L/2 < x_0 < L/2$  and a discretization of the interval  $[-L/2, L/2]$ ,  $\{\chi_0, \chi_1, \dots, \chi_n\}$ .
- 2: Discretize the differential operators  $\mathbf{A}$  and the adjoint  $\mathbf{A}^*$  where

$$\mathbf{A} \begin{pmatrix} u_1 \\ u_2 \end{pmatrix} = \left\{ \begin{bmatrix} v \frac{d}{dx} & 0 \\ 0 & -v \frac{d}{dx} \end{bmatrix} + F(x) \begin{bmatrix} -1 & 1 \\ 1 & -1 \end{bmatrix} \right\} \begin{pmatrix} u_1(x) \\ u_2(x) \end{pmatrix},$$

$$\mathbf{A}^* \begin{pmatrix} p_1 \\ p_2 \end{pmatrix} = \left\{ \begin{bmatrix} -v \frac{d}{dx} & 0 \\ 0 & v \frac{d}{dx} \end{bmatrix} + F(x) \begin{bmatrix} -1 & 1 \\ 1 & -1 \end{bmatrix} \right\} \begin{pmatrix} p_1(x) \\ p_2(x) \end{pmatrix}.$$

Note that  $\mathbf{A}$  must account for the boundary conditions  $u_1(L/2) = 0$  and  $u_2(-L/2) = 0$  respectively and  $\mathbf{A}^*$  must account for the adjoint boundary conditions  $p_1(-L/2) = 0$  and  $p_2(L/2) = 0$ .

- 3: Compute  $s_1, \dots, s_N$ , the first  $N$  complex eigenvalues of  $\mathbf{A}$  with smallest absolute value.
- 4: Compute the corresponding  $N$  eigenvectors of  $\mathbf{u}_1, \dots, \mathbf{u}_N$  of  $\mathbf{A}$  and  $\mathbf{p}_1, \dots, \mathbf{p}_N$  of  $\mathbf{A}^*$ .
- 5: Compute the inner products  $D_m = \int_{-L/2}^{L/2} \mathbf{p}_m^*(x) \mathbf{u}_m(x) dx$  for  $m = 1, \dots, N$ .
- 6: Compute the functions  $h_m^{(1)}(t)$  and  $h_m^{(2)}(t)$  in (15) and (16) for  $m = 1, \dots, N$ .
- 7: Compute  $a_1(x)$  and  $a_2(x)$  in (17) and (18).
- 8: Compute

$$\mathbf{Z}(x_0, t) = - \sum_{m=1}^N \frac{\mathbf{u}_m(x_0)}{s_m D_m} [h_m^{(1)}(t) + h_m^{(2)}(t)], \quad (21)$$

as the  $N$ -term approximation to (14). If  $x_0$  does not coincide with a grid point  $\chi_j$ , use interpolation to find  $\mathbf{u}_m(x_0)$ .

- 9: Compute  $W_1(x_0, t)$  and  $W_2(x_0, t)$  by adding discontinuities of strength  $a_1(x_0)$  and  $a_2(x_0)$  at  $t = -x_0/v + L/(2v)$  and  $t = x_0/v + L/(2v)$  respectively to  $Z_1$  and  $Z_2$ : see eqs. (12) and (13).
  - 10: Output  $W_1(x_0, t)$  and  $W_2(x_0, t)$ .
-

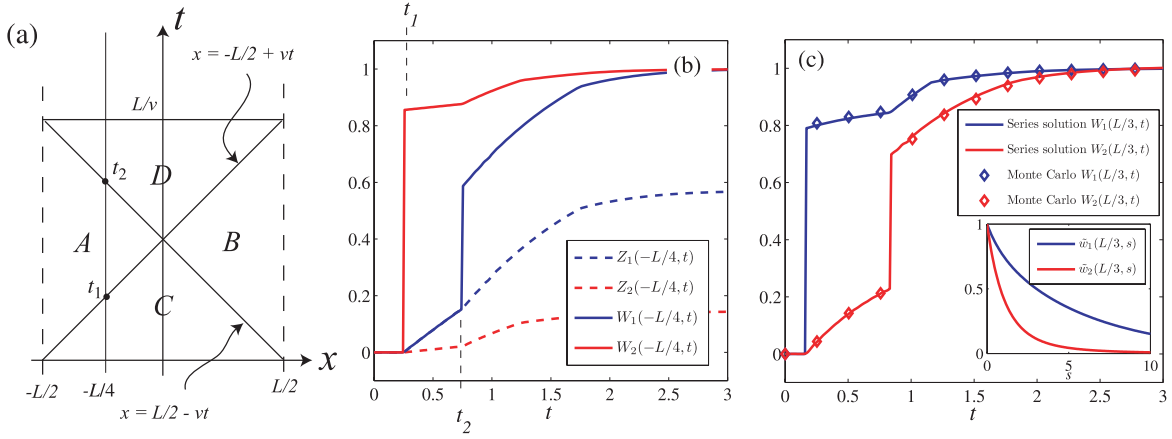


Figure 1: (a) Propagation of discontinuities of (1)-(3) in the  $x$ - $t$  plane. The solution  $w_1(x, t)$  is formally infinite on  $x = L/2 - vt$  while  $w_2(x, t)$  is infinite on  $x = -L/2 + vt$ . These singularities give rise to discontinuities in  $W_1$  and  $W_2$  that can be seen in (b,c). (b) Numerical computation of cumulative probability densities (cdfs)  $W_{1,2}(x_0 = -L/4, t)$  and auxiliary functions  $Z_{1,2}(x_0 = -L/4, t)$  computed through (14) and Algorithm 2 using using 101 Chebyshev grid points and 51 eigenfunctions  $\mathbf{u}_1, \mathbf{u}_2, \dots, \mathbf{u}_{51}$ . (c) Numerical computation of cdfs  $W_{1,2}(x_0 = L/3, t)$  (solid) along with results from Monte Carlo simulations (diamond). Inset shows Laplace-transformed probability densities  $\tilde{w}_{1,2}(x_0 = L/3, s)$ . Common parameters in (b,c) are  $v = 1$ ,  $F(y) = 1 + y$  and  $L = 1$ .

151 integrals (15) and (16) for  $0 < t < L/v$ . The strength of this numerical method is that no  
 152 integration in time is required to find  $W_{1,2}(x_0, t)$  and the method allows quick evaluation of  
 153 the cdfs at one fixed value of  $x = x_0$ . Its weakness is that many terms are usually required  
 154 ( $\gtrsim 100$ ) in the expansion to obtain accurate results when  $x_0$  is close to  $\pm L/2$ . Furthermore  
 155 we found that when  $x_0 = \pm L/2$ , the expansion (14) converged to a discontinuous function,  
 156 giving  $W_{1,2}(x_0, t) > 1$  as  $t \rightarrow \infty$ ; hence the properties of the series (14) still require further  
 157 investigation at the domain boundaries.

158 Another important reason for separating out  $W_1$  and  $W_2$  into continuous and discontin-  
 159 uous components is to avoid Gibbs oscillations when solving for  $\mathbf{Z}(x, t)$  as superpositions of  
 160 eigenfunctions  $\mathbf{u}_n$ . These oscillations would introduce large errors into the solution to the  
 161 forward problem (5)-(8) and therefore hinder the solution of the inverse problem.

162 *Proof of Theorem 1.* Upon substituting (12), (13) into (5), (6), we find that  $Z_{1,2}(x, t)$  satisfy

$$\frac{\partial Z_1}{\partial t} - v \frac{\partial Z_1}{\partial x} - F(x)(Z_2 - Z_1) = a_2(x)F(x)H[t - x/v - L/(2v)], \quad (22)$$

$$\frac{\partial Z_2}{\partial t} + v \frac{\partial Z_2}{\partial x} - F(x)(Z_1 - Z_2) = a_1(x)F(x)H[t + x/v - L/(2v)], \quad (23)$$

163 subject to the *homogeneous* boundary conditions  $Z_1(L/2, t) = 0$ ,  $Z_2(-L/2, t) = 0$  and initial  
 164 conditions  $Z_1(x, 0) = 0$ ,  $Z_2(x, 0) = 0$  and  $a_{1,2}$  are defined by (17) and (18). We now find a



165 series representation for  $Z_{1,2}(x, t)$ . After taking Laplace transforms of (22) and (23), we find  
 166 that  $\tilde{\mathbf{Z}}(x, s) = \left[ \tilde{Z}_1(x, s), \tilde{Z}_2(x, s) \right]^T$  satisfies

$$\begin{aligned} (\mathbf{A} - s\mathbf{I})\tilde{\mathbf{Z}}(x, s) &= -\frac{\tilde{\mathbf{N}}(x, s)}{s}, \\ \tilde{\mathbf{N}}(x, s) &= F(x) \begin{bmatrix} a_2(x)e^{-\left(\frac{L}{2v} + \frac{x}{v}\right)s} \\ a_1(x)e^{-\left(\frac{L}{2v} - \frac{x}{v}\right)s} \end{bmatrix}. \end{aligned}$$

167 with boundary conditions  $\tilde{Z}_1(L/2, s) = 0, \tilde{Z}_2(-L/2, s) = 0$ . Eq. (24) has a solution of the  
 168 form

$$\tilde{\mathbf{Z}}(x, s) = \sum_{n=1}^{\infty} \frac{c_n(s)\mathbf{u}_n(x)}{s - s_n}, \quad (24)$$

169 where the vector eigenfunctions  $\mathbf{u}_n(x) \in \mathbb{C}^2$  satisfy  $\mathbf{A}\mathbf{u}_n = s_n\mathbf{u}_n$  for eigenvalues  $s_n \in \mathbb{C}$ . As an  
 170 aside, when  $F(x) = F_0$  is a constant, one can show that the eigenfunctions are proportional  
 171 to  $[-(\alpha^2 + \lambda_n^2)^{1/2} \sinh \lambda_n(x + 1/2) + \lambda_n \cosh \lambda_n(x + 1/2), \alpha \sinh \lambda_n(x + 1/2)]^T$  with  $\alpha \equiv F_0L/v$ ,  
 172 the  $\lambda_n \in \mathbb{C}$  satisfy the transcendental equation  $-(\alpha^2 + \lambda_n^2)^{1/2} \tanh \lambda_n + \lambda_n = 0$ , and the  
 173 eigenvalues are given by  $s_n = -\alpha - (\alpha^2 + \lambda_n^2)^{1/2}$ .

Recall that if  $\{\mathbf{u}_n\}$  are the eigenfunctions of  $\mathbf{A}$  and  $\{\mathbf{p}_m\}$  are the eigenfunctions of the  
 adjoint operator  $\mathbf{A}^*$ , then  $\langle \mathbf{p}_m, \mathbf{u}_n \rangle = 0$  unless  $m = n$ . Substituting (24) into (24), left-  
 multiplying both sides of by  $\mathbf{p}_m^*$  and integrating, we find that

$$c_n(s) = \frac{\langle \mathbf{p}_m(x), \tilde{\mathbf{N}}(x, s) \rangle}{sD_m},$$

174 where  $D_m$  is defined by (19). (One cannot obtain  $c_n$  by invoking orthogonality of  $\{\mathbf{u}_n\}$  since  
 175  $\mathbf{A}$  is not self-adjoint.) We now take the inverse Laplace transform of (24) and switch the  
 176 order of integration to obtain the continuous parts of the cumulative density functions (cdfs):

$$\begin{aligned} \mathbf{Z}(x, t) &= \sum_{m=1}^{\infty} \frac{\mathbf{u}_m(x)}{D_m} \left\{ \int_{-L/2}^{L/2} dy p_m^{(1)*}(y) a_2(y) F(y) \int_{\gamma-i\infty}^{\gamma+i\infty} \frac{ds}{2\pi i} \frac{e^{(t-\frac{y}{v}-\frac{L}{2v})s}}{s(s-s_m)} + \right. \\ &\quad \left. \int_{-L/2}^{L/2} dy p_m^{(2)*}(y) a_1(y) F(y) \int_{\gamma-i\infty}^{\gamma+i\infty} \frac{ds}{2\pi i} \frac{e^{(t+\frac{y}{v}-\frac{L}{2v})s}}{s(s-s_m)} \right\}, \quad \text{Re}\gamma > 0, \\ &= -\sum_{m=1}^{\infty} \frac{\mathbf{u}_m(x)}{s_m D_m} [h_m^{(1)}(t) + h_m^{(2)}(t)]. \end{aligned}$$

177 where  $h_m^{(1)}(t)$  and  $h_m^{(2)}(t)$  are given by eqs. (15) and (16) respectively. □

## 178 2.2 Monte-Carlo simulation using Rejection-Acceptance

179 We now give details of our Monte-Carlo method in Algorithm 3. This method can be used to  
 180 simulate a broadwell particle with spatially dependent velocity, even though for our inverse

181 problem, the particles always have constant velocity. The method is based on the Rejection-  
 182 Acceptance method [3], a common method for drawing random variables from a pdf whose  
 183 functional form is known, but non-standard. We note four important points about the  
 184 algorithm.

- 185 1. The algorithm samples from  $w_1(y_0, t)$  or  $w_2(y_0, t)$  depending on the initial velocity: see  
 186 eqs. (27).
- 187 2. The algorithm generates random variables for the time periods in between the state  
 188 transitions  $\theta$  (the ‘‘flip times’’). For a Broadwell process with a constant transition  
 189 rate, the flip times are exponentially distributed. For a *spatially-dependent* transition  
 190 rate  $F(y)$ , the flip time  $\theta \equiv t_{j+1} - t_j$  is distributed according to

$$\begin{aligned} \theta \sim Q(t) &\equiv F[y(t)] \exp[-p(t)], \\ p(t) &= \int_0^t F[y(t')] dt', \end{aligned} \quad (25)$$

where the position of the particle satisfies  $dy(t)/dt = v(y)$ . We sample from  $Q(t)$  using a Rejection-Acceptance method [3]: suppose there exist constants  $F_{\min}$  and  $F_{\max}$  satisfying  $0 < F_{\min} \leq F(y) \leq F_{\max} < \infty$  for  $-L/2 < y < L/2$ . Then

$$Q(t) \leq CF_{\min} \exp(-F_{\min}t) \equiv P(t),$$

191 where  $C = F_{\max}/F_{\min}$  and so an exponential distribution can be used as an envelope  
 192 function.

- 193 3. Once the flip time  $\theta$  is generated, the flip position  $y_{j+1}$  can be found by solving  
 194  $\int_{y_j}^{y_{j+1}} v^{-1}(y)dy = \theta$ . This integral could be expensive to calculate if it has to be done  
 195 many times. Also, every evaluation of  $Q(t)$  requires computing the integral  $p(t)$  in (25).  
 196 Both of these issues are handled simultaneously in our algorithm through the solution  
 197 of the pair of ordinary differential equations (26)-(??). For the special case where  $v$  is a  
 198 constant, (26) and (27) should be replaced with  $dp/dt = F(y_j + vt)$  and  $y(t) = y_j + vt$ .
- 199 4. When solving the differential equations (26) and (27),  $F$  may have to be evaluated  
 200 outside of the interval  $[-L/2, L/2]$ . Because the form of  $F(y)$  outside  $[-L/2, L/2]$  does  
 201 not affect the exit time, we simply take  $F(y) = F(L/2)$  for  $y > L/2$  and  $F(y) =$   
 202  $F(-L/2)$  for  $y < -L/2$ .

203 Figure 2 shows the probability density functions  $w_1(0, t)$  generated by the algorithm for  
 204 two different  $F(x)$  when  $v(x) = \text{constant}$ . By definition,  $w_1$  is the exit time density for a  
 205 particle that initially has velocity  $v > 0$ . Therefore the solution  $w_1(x, t)$  in (1) contains delta  
 206 functions that correspond to an immediate particle exit at a time  $t_c \equiv (L/2 - x)/v$ . The  
 207 reason is if  $t$  is the particle exit time and  $\theta$  is the time before the *first* state transition, then

$$P(t = t_c) = P(\theta \geq t_c) = \int_{t_c}^{\infty} Q(t') dt' > 0. \quad (28)$$

---

**Algorithm 3** Generating exit times from a Broadwell process
 

---

- 1: Require: an interval size  $L$ , a starting position  $-L/2 \leq y_0 \leq L/2$ , functions  $F(y), v(y) \in C(-\infty, +\infty)$ ,  $F_{\min}, F_{\max} > 0$  where  $F_{\min} \leq F(y) \leq F_{\max}$  for  $y \in [-L/2, L/2]$ .
- 2: Let  $P(t) \equiv F_{\max} \exp(-F_{\min} t)$ .
- 3: Set  $j = 0$  and  $t_j = 0$ .
- 4: **while**  $-L/2 < y_j < L/2$  **do**
- 5:   Draw  $\theta \sim \exp(F_{\min})$
- 6:   Compute  $p(\theta)$  and  $y(\theta)$  by numerically solving

$$\frac{dp(t)}{dt} = F(y), \tag{26}$$

$$\frac{dy(t)}{dt} = \begin{cases} (-1)^j v(y), & \{\text{for positive velocity at } t = 0\} \\ (-1)^{j+1} v(y), & \{\text{for negative velocity at } t = 0\} \end{cases} \tag{27}$$

on  $t \in [0, \theta]$ , subject to initial conditions  $p(0) = 0$  and  $y(0) = y_j$ .

- 7:   Set  $Q(\theta) = F[y(\theta)] \exp[-p(\theta)]$
  - 8:   Draw  $\rho \sim U(0, 1)$
  - 9:   **if**  $\rho < Q(\theta)/P(\theta)$  **then**
  - 10:      $j \leftarrow j + 1$  {acceptance}
  - 11:     Set  $y_j = y(\theta)$  and  $t_j = t_{j-1} + \theta$
  - 12:     Goto 4
  - 13:   **else**
  - 14:     Goto 5 {rejection}
  - 15:   **end if**
  - 16: **end while**{Particle has left interval}
  - 17: **if**  $y_j > L/2$  **then**
  - 18:   Output the exit time as  $t_j + \int_{y_j}^{L/2} v^{-1}(y) dy$ .
  - 19: **else**
  - 20:   Output the exit time as  $t_j + \int_{y_j}^{-L/2} (-v^{-1}(y)) dy$ .
  - 21: **end if**
-

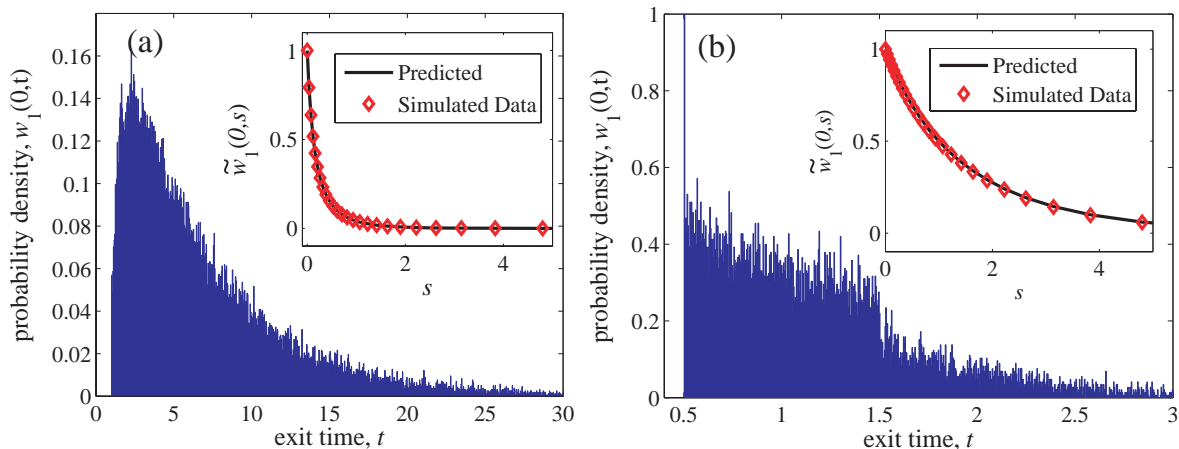


Figure 2: Simulated exit times of a Broadwell process. Although probability densities are shown here, cumulative density functions are used to infer the flip rate function. (a)  $F(x) = 10x^3 + 5e^x + 1$ ,  $v = 1/2$  (b)  $F(x) = 1 + x^2$ ,  $v = 1$ . Insets show Laplace-transformed data. Solid line: solution to (9), (10). Red diamonds: Laplace transform of histogram data. The number of realizations was  $N = 40,000$  in each case.

208 Hence the probability distribution of the exit times will always contain point masses (delta  
 209 functions) of probability located at  $t = t_c$  [20]. In Fig. 2(b) a numerical approximation of  
 210 this delta function can be seen. The height of this “spike” is controlled by the size of the  
 211 bins used when creating the histogram and becomes unbounded as the bin size tends to zero  
 212 and the number of trials tends to infinity. These delta distributions are always present in the  
 213 exact solution but they may not always be visible in the numerical solution if the number of  
 214 trials is small or the bin size is large; see Fig. 2(a) for example.

### 215 2.2.1 Generation of noisy distributions from a finite number of exit times

216 We always use Algorithm 3 to generate two sets of  $N$  exit times  $\{\tau_j^{(1)}\}$  and  $\{\tau_j^{(2)}\}$ . With  
 217 this notation,  $\tau_j^{(i)}$  ( $1 \leq j \leq N$ ,  $i = 1, 2$ ) is the  $j$ th exit time conditioned on the particle  
 218 having initial velocity  $(-1)^{i+1}v$ . Assuming that  $\{\tau_j^{(1)}\}$  and  $\{\tau_j^{(2)}\}$  are sorted in ascending  
 219 order, noisy cumulative densities  $W_{1,\text{data}}(t)$  and  $W_{2,\text{data}}(t)$  are computed as

$$W_{i,\text{data}}(t) = \begin{cases} 0 & \text{if } t < \tau_1^{(i)}, \\ \frac{m}{N} & \text{if } \tau_1^{(i)} < t < \tau_N^{(i)}, \\ 1 & \text{if } t \geq \tau_N^{(i)}, \end{cases} \quad (29)$$

220 where  $m$  is the unique index satisfying  $\tau_m^{(i)} < t < \tau_{m+1}^{(i)}$ .

221 The noisy Laplace transform of a finite number of exit times is calculated through

$$\tilde{w}_{j,\text{data}}(s) = \begin{cases} \int_0^\infty e^{-st} \frac{dW_{j,\text{data}}(t)}{dt} dt = s\tilde{W}_{j,\text{data}}(s), & s > 0, \\ 1, & s = 0, \end{cases} \quad (30)$$

222 where

$$\tilde{W}_{j,\text{data}}(s) = \int_0^\infty e^{-st} W_{j,\text{data}}(t) dt = \int_0^1 e^{-st[\eta]} W_{j,\text{data}}(t[\eta]) \frac{d\eta}{(1-\eta)^2}, \quad (31)$$

223 where  $j = 1, 2$  and  $t[\eta] = \eta/(1-\eta)$ . We avoid ‘‘binning’’ when calculating  $\tilde{w}_{j,\text{data}}$ , since this  
 224 introduces a corresponding discretization error. The integral in (31) can be calculated using  
 225 the trapezium rule on equally spaced abscissae in  $\eta$ .

## 226 2.3 Projection method to solve inverse problem

227 We now briefly describe our algorithms for reconstructing the flip rate function  $F(x)$  from  
 228 the two distributions of exit times  $w_{1,\text{data}}(t)$  and  $w_{2,\text{data}}(t)$ . These distributions can come  
 229 from simulating the Broadwell process directly through Algorithm 3 or through a one-time  
 230 solution of the forward problems (9)-(11) or (5)-(8). We implement two related algorithms.  
 231 The first method uses the exit time data directly ( $t$ -method) and the second method uses  
 232 Laplace-transformed exit time data ( $s$ -method). Pseudocode for the two methods is given in  
 233 Algorithms 4 and 5.

234 In both methods, we represent the trial flip rate function  $F_M(x)$  and the target flip rate  
 235 function  $F^*(x)$  as linear combination of Legendre polynomials on  $[-L/2, L/2]$ :

$$F_M(x) = \sum_{j=0}^{M-1} a_j \phi_j(x), \quad (32)$$

236 For example,  $\phi_0(x) = 1$ ,  $\phi_1(x) = 2x/L$ ,  $\phi_2(x) = 6\left(\frac{x}{L}\right)^2 - \frac{1}{2}$ .

237 Our aim is to find coefficients  $a_1, \dots, a_M$  to minimize the objective functions for the  
 238  $t$ -method and  $s$ -methods,  $\Pi_1$  and  $\Pi_2$  respectively. These take the form

$$\begin{aligned} \Pi_1(\mathbf{a}) &= \int_0^{L/v} |W_1(x_0, t; \mathbf{a}) - W_{1,\text{data}}(x_0, t)|^2 dt + \int_0^{L/v} |W_2(x_0, t; \mathbf{a}) - W_{2,\text{data}}(x_0, t)|^2 dt, \\ \Pi_2(\mathbf{a}) &= \int_0^\infty |\tilde{w}_1(x_0, s; \mathbf{a}) - \tilde{w}_{1,\text{data}}(x_0, s)|^2 ds + \int_0^\infty |\tilde{w}_2(x_0, s; \mathbf{a}) - \tilde{w}_{2,\text{data}}(x_0, s)|^2 ds. \end{aligned}$$

239 The data sets  $W_{j,\text{data}}(x_0, t)$ ,  $\tilde{w}_{j,\text{data}}(x_0, s)$  associated with  $F^*(x)$  can be computed from indi-  
 240 vidual exit times using (29) and (30) respectively.

241 Minimization of  $\Pi_1$  and  $\Pi_2$  with respect to  $\mathbf{a}$  was performed using the Matlab rou-  
 242 tines `fminunc.m` and `lsqnonlin.m` for the  $t$  and  $s$  methods respectively, with the tolerances  
 243 `TolFun` and `TolX` set to  $10^{-14}$ . The initial guess for the coefficients was always  $a_j = 1$   
 244 for  $j = 1, \dots, M$ , unless otherwise stated. The minimizing coefficients  $\hat{a}_j$  then define the  
 245 reconstructed flip rate through  $\hat{F}(x) = \sum_{j=1}^N \hat{a}_j \phi_j(x)$ .

246 An obvious limitation of the projection method is that the method does not converge for  
 247 non-polynomial  $F^*$  and polynomial  $F^*$  with degree  $> M$ . However, as we shall see in section  
 248 3, the method may still be used to find reasonable approximations in these cases.

---

**Algorithm 4** Reconstruction of flip rate coefficients using the  $t$ -method

---

- 1: Require: An integer  $M$ , an interval length  $L$ , target flip rate function  $F^*(x)$ , a particle speed  $v > 0$ , a starting position  $-L/2 < x_0 < L/2$  and the first  $M$  legendre polynomials on  $(-L/2, L/2)$ ,  $\phi_1, \dots, \phi_M$  (see text for details).
- 2: Generate noisy cdfs of the exit time  $W_{1,\text{data}}(x_0, t)$  and  $W_{2,\text{data}}(x_0, t)$  for  $F^*(x)$  using Algorithm 3.
- 3: For a given  $\mathbf{a} = (a_0, a_1, \dots, a_{M-1}) \in \mathbb{R}^M$ , define  $F_M(x) = \sum_{j=0}^{M-1} a_j \phi_j(x)$ . Let  $W_{1,2}(x_0, t; \mathbf{a})$  be the solution to the forward problem (5)-(8) with  $F = F_M$ , calculated using Algorithm 2.
- 4: Find  $\mathbf{a} = \hat{\mathbf{a}}$  that minimizes

$$\Pi_1(\mathbf{a}) = \int_0^{L/v} |W_1(x_0, t; \mathbf{a}) - W_{1,\text{data}}(x_0, t)|^2 dt + \int_0^{L/v} |W_2(x_0, t; \mathbf{a}) - W_{2,\text{data}}(x_0, t)|^2 dt. \quad (33)$$

Integrating through discontinuities can be avoided by noting that  $W_{1,2}(x, t) = 0$  when  $t < \min(\frac{L}{2v} - \frac{x}{v}, \frac{x}{v} + \frac{L}{2v})$ . The lower limits of integration in (33) can be replaced with  $(\frac{L}{2v} - \frac{x_0}{v})^+$  when  $0 \leq x_0 < L/2$  and  $(\frac{x_0}{v} + \frac{L}{2v})^+$  when  $-L/2 < x_0 \leq 0$ .

- 5: Output  $\hat{F}(x) \equiv \sum_{j=0}^{M-1} \hat{a}_j \phi_j(x)$  as the estimate of the flip rate function for the exit time distributions  $W_{1,\text{data}}(x_0, t)$  and  $W_{2,\text{data}}(x_0, t)$ .
- 

## 249 3 Results and Discussion

### 250 Flip Rate Reconstruction

251 We used the projection algorithm discussed in section 2.3 to reconstruct flip rate functions  
 252 from data generated using Monte Carlo simulation (see section 2.2). In the following discus-  
 253 sion, let  $N$  be the number of exit times for each initial velocity  $+v, -v$ , so that the total  
 254 number of exit times is always  $2N$ . We also take the starting position  $x_0 = 0$ , interval length  
 255  $L = 1$  and particle speed  $v = 1$  unless otherwise stated.

256 For Fig. 3, we reconstruct some “structurally simple” smooth functions that have few  
 257 extrema within  $(-L/2, L/2)$  and find that the accuracy of the reconstructions improves as  
 258 the noise in the data decreases. For the “ $N = \infty$ ” cases, artificial, noiseless data is generated  
 259 by solving the forward problems eqs. (5)-(8) and (9)-(11) with  $F = F^*$ . Panels (a-f) indicate  
 260 that for a given  $N$ , the  $t$ -method generally outperforms the  $s$ -method since the associated  
 261 errors are smaller. In (a,b) we reconstruct a cubic polynomial by recovering  $M = 4$  Legendre  
 262 coefficients. In (c,d) we attempt to reconstruct a transcendental function by representing  
 263  $F^*(x)$  with  $M = 5$  coefficients. Although  $\|F_M - F^*\|_\infty \rightarrow 0$  as the noise decreases, we are  
 264 still able to find a reasonable approximation  $F_M$  so that  $\|F_M - F^*\|_\infty$  is not too large. The  $s$ -  
 265 method converges to the correct solution for perfect data but the inclusion of a small amount

---

**Algorithm 5** Reconstruction of flip rate coefficients using the  $s$ -method

---

- 1: Require: An integer  $M$ , an interval length  $L$ , a target flip rate function  $F^*(x)$ , a particle speed  $v > 0$  and a starting position  $-L/2 < x_0 < L/2$  and the first  $M$  Legendre polynomial on  $(-L/2, L/2)$ ,  $\phi_1, \dots, \phi_M$  (see text for details).
- 2: Use  $F^*(x)$  to generate Laplace-transformed exit time pdfs  $\tilde{w}_{1,\text{data}}(x_0, s)$  and  $\tilde{w}_{2,\text{data}}(x_0, s)$  through Algorithm 3.
- 3: For a given  $\mathbf{a} \in \mathbb{R}^M$ , let  $\tilde{w}_{1,2}(x_0, s; \mathbf{a})$  be the solution to the forward problem (9)-(11) calculated using Algorithm 1 with flip rate function defined by  $\mathbf{a} = \{a_0, a_2, \dots, a_{M-1}\}$ :

$$F_M(x) = \sum_{j=0}^{M-1} a_j \phi_j(x).$$

- 4: Find  $\mathbf{a} = \hat{\mathbf{a}}$  that minimizes

$$\Pi_2(\mathbf{a}) = \int_0^\infty |\tilde{w}_1(x_0, s; \mathbf{a}) - \tilde{w}_{1,\text{data}}(x_0, s)|^2 ds + \int_0^\infty |\tilde{w}_2(x_0, s; \mathbf{a}) - \tilde{w}_{2,\text{data}}(x_0, s)|^2 ds, \quad (34)$$

The integral in (34) is calculated using using a change of variable  $s[\xi] = \xi/(1 - \xi)$  so that

$$\Pi_2 = \sum_{j=1}^2 \int_0^1 [\tilde{w}_j(x_0, s[\xi], \mathbf{a}) - \tilde{w}_{j,\text{data}}(x_0, s[\xi])]^2 \frac{d\xi}{(1 - \xi)^2},$$

which can be computed using the trapezium rule on equally spaced abscissae on  $[0,1]$ .

- 5: Output  $\hat{F}(x) \equiv \sum_{j=0}^{M-1} \hat{a}_j \phi_j(x)$  as the estimate of the flip rate function for the exit time distributions  $\tilde{w}_1(x_0, s)$  and  $\tilde{w}_2(x_0, s)$ .
-

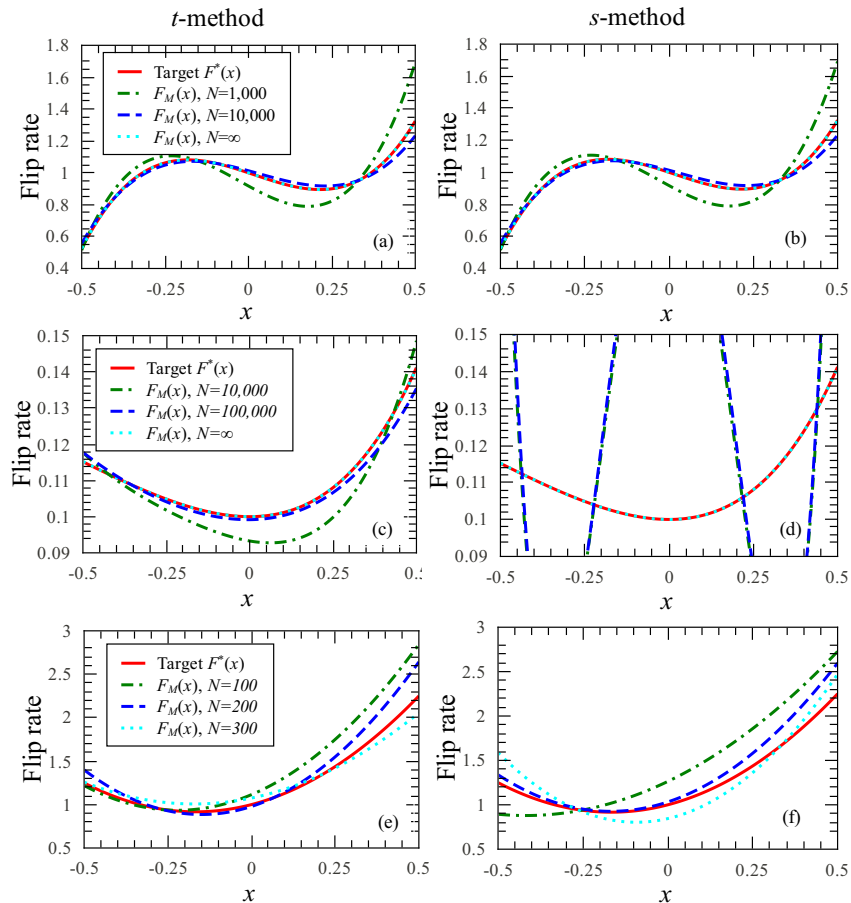


Figure 3: Reconstructed approximations to flip rate functions  $F^*(x)$  from noisy exit time data. (a,b)  $F^*(x) = 1 - 0.7x - 0.3x^2 + 6x^3$ ,  $M = 4$ ; (c,d)  $F^*(x) = x^2 e^{-x}/10 + 1/10$ ,  $M = 5$ ; (e,f)  $F^*(x) = 1 + x + 3x^2$ ,  $M = 3$ . The  $t$ -method was used in the left panels and the  $s$ -method was used in the right panels.  $N = \infty$  corresponds to perfect, noiseless data, which is generated by solving the forward problems (5)-(8) and (9)-(11).

266 of noise renders the method unstable, resulting in a large error. This kind of behavior also  
 267 occurs with the  $t$ -method when  $M \gtrsim 5$  and is typical in many ill-posed problems (see below).  
 268 In (e) and (f), we reconstruct flip rate functions from a relatively small number of exit times  
 269 by taking  $M = 3$  basis functions; however, smaller  $M$  restricts the range of admissible target  
 270 functions.

271 If we have no *a-priori* knowledge on  $F^*(x)$  (e.g. it may be a high-degree polynomial,  
 272 have many extrema or be discontinuous), our method may not capture  $F^*(x)$  accurately.  
 273 For our method to be successful, it is important that we know beforehand that  $F^*(x)$  is  
 274 smooth and structurally not too complex. Increasing the number of basis functions  $M$  in-  
 275 creases the range of functions we can accurately represent. Providing  $F^*$  is smooth enough,  
 276 it can always be represented through its Taylor series and our method strives to capture its  
 277 first  $M$  coefficients. Ideally, we would like  $M$  to be as large as possible to represent any



$M$	$\kappa_t$	$\kappa_s$
2	$5.3 \times 10^2$	$3.1 \times 10^2$
3	$1.0 \times 10^4$	$3.3 \times 10^4$
4	$1.4 \times 10^5$	$3.5 \times 10^6$
5	$1.0 \times 10^6$	$1.6 \times 10^8$

Table 1: Local condition numbers  $\kappa_s$  and  $\kappa_t$  for  $F^*(x) = 1 + x$  corresponding to the objective functions (34) and (33) respectively.  $M$  denotes the number of basis functions used in (32).

$M$	$\kappa_t$	$\kappa_s$
3	$5.0 \times 10^5$	$1.8 \times 10^5$
4	$3.5 \times 10^6$	$1.6 \times 10^7$
5	$6.7 \times 10^6$	$5.2 \times 10^8$

Table 2: Local condition numbers for  $F^*(x) = 1 - x + x^2$ : see Table 1 for details.

278  $F^*(x) \in C^\infty(-L/2, L/2)$ . However in practice it is difficult to reliably reconstruct  $F^*(x)$   
279 (even polynomials) when  $M \gtrsim 5$ . The reason, which is common with all projection methods  
280 [11, 18], is that as the finite-dimensional approximation to  $F^*(x)$  improves with  $M \rightarrow \infty$ , the  
281 method becomes more unstable due to ill-posedness. In this limit, minimizing the objective  
282 functions (33), (34) is prone to large errors.

283

### 284 Instability of Projection Method

285 Numerically, the instability discussed above may be quantified by examining the condition  
286 number of the objective function near its minimum. Specifically, we study the Hessian  
287 (matrix of second partial derivatives) of the objective functions  $\Pi_1$  and  $\Pi_2$  in (33) and (34)  
288 with respect to the coefficients  $a_j$ ,  $j = 0, \dots, M - 1$ :

$$H_{ij}^{(1)} \equiv \frac{\partial^2 \Pi_1}{\partial a_i \partial a_j} \Big|_{a_i=a_i^*, a_j=a_j^*}, \quad H_{ij}^{(2)} \equiv \frac{\partial^2 \Pi_2}{\partial a_i \partial a_j} \Big|_{a_i=a_i^*, a_j=a_j^*}, \quad (35)$$

289 for  $i, j = 0, \dots, M - 1$ . In (35),  $a_i^*$  are the target coefficients of a polynomial flip rate function:  
290  $F^*(x) = \sum_{i=0}^{M-1} a_i^* \phi_i(x)$ . The condition number of a matrix  $A$  is defined as the ratio of its  
291 largest eigenvalue to its smallest:  $\kappa = \lambda_{\max}(A)/\lambda_{\min}(A)$ . Since the eigenvalues represent the  
292 principle curvatures of  $\Pi_{1,2}$  at the point  $\mathbf{a}^*$ , they are always positive; a very large condition  
293 number indicates that  $\Pi_1$  or  $\Pi_2$  is locally very flat at  $\mathbf{a} = \mathbf{a}^*$  and finding  $\mathbf{a}^*$  numerically  
294 is prone to errors. On the other hand, a moderate-sized condition number indicates only a  
295 small difference in curvatures near  $\mathbf{a}^*$  and so finding the minimum numerically should not be  
296 difficult. Tables 1 and 2 show that both condition numbers for the  $t$ - and  $s$ -methods grow  
297 exponentially as the number of basis functions  $M$  increases. For  $M = 5$  basis functions,  
298 the condition numbers for the  $t$ -method are consistently two orders of magnitude smaller  
299 than those for the  $s$ -method. This suggests that fitting to the exit time data directly (as  
300 opposed to its Laplace transform) leads to more effective algorithms and better estimates  
301 for the flip rate function. This is confirmed in our numerical experiments since occasionally  
302 the  $t$ -method is able to recover  $M = 5$  coefficients of a quartic polynomial  $F(x)$ , but the  
303  $s$ -method is seldom able to do so.

304

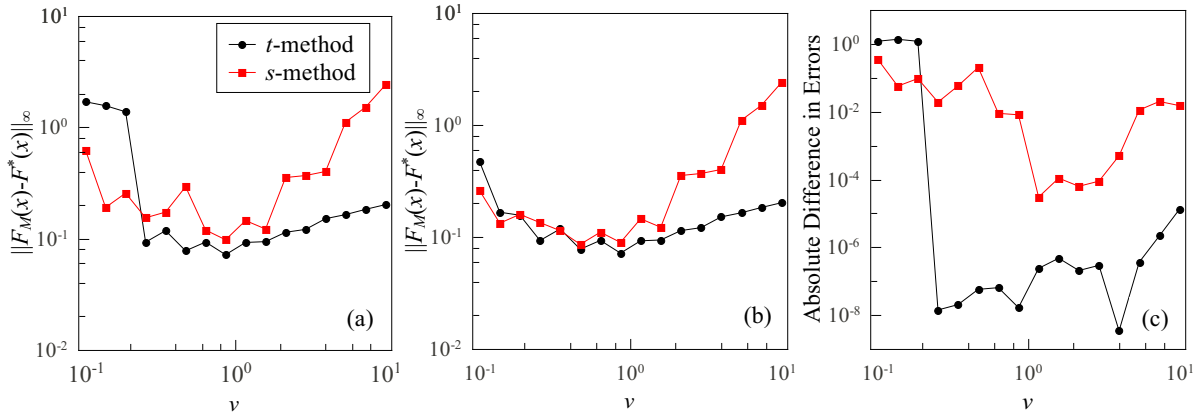


Figure 4: Error in reconstructed flip rate as a function of particle velocity. Each point is an average over 10 sets of  $2N = 20,000$  exit times. Target flip rate  $F^*(x) = \frac{9}{4}x^2 - \frac{3}{4}x + \frac{9}{16}$ , corresponding to target coefficients  $\mathbf{a}^* = [0.75, -0.375, 0.375, 0]$ . Initial guesses are (a)  $\mathbf{a} = [1, 1, 1, 1]$ , (b)  $\mathbf{a} = [0.76, -0.385, 0.365, 0.01]$ . The same exit times were used for both (a) and (b). The difference in the errors is shown in (c).

### Sensitivity of Reconstruction to Advection Speed

We also explore the accuracy our reconstruction for different advection speeds  $v$ , given a fixed number of exit times when  $F^*(x)$  is a polynomial of degree  $\leq M$ . In Fig. 4, we see that, for both methods, when the velocity is either much less or much larger than unity, the associated error is large. (Although the upper limit of the objective function (33) depends on the value of  $v$  used, we checked that the non-monotonic behavior in  $\|F_M - F^*\|_\infty$  was not sensitive to the upper limit of integration.)

In practice, there are always two sources of error in the reconstruction of  $F^*$ : the first is from noise in the data and the second stems from the minimization procedure itself:

$$\text{Total error} = \text{error from noise in data} + \text{error from minimization.} \quad (36)$$

If the minimization of the objective functions (33) or (34) was achieved with zero error, noisy exit times would still produce an error in the reconstructed  $F$ . On the other hand, for noiseless data, the flat minima and large condition numbers discussed above would produce an erroneous  $F$  from the minimization. It is hard to separate the two types of error in (36), but some insight can be gained by comparing Figs. 4 (a) and (b) which differ only in the starting values for the coefficients  $a_0, \dots, a_{M-1}$ ; in particular the exit times for each value of  $v$  for each figure are identical. When we move the initial guess for the coefficients closer to their target values in (b), we greatly reduce the error in minimization since the accuracy of minimization algorithms depends on the quality of the initial guess. Therefore, the error in (b) comes mainly from *noise in the data*. Since the exit times were identical for (a) and (b), the difference of the errors in (a) and (b) – shown in (c) – represents the *error from minimization* which is associated with large condition numbers and flat extrema. We note that the error from minimization from the *s*-method is much larger than the corresponding error from the *t*-method for a wide range of  $v$  values.

328 When the dominant error stems from noise in the data (as is the case in Fig. 4(b)), we  
 329 can understand why  $v = O(1)$  provides the most accurate reconstruction by analyzing how  
 330 well the Monte Carlo simulations approximate the moments of the exit time distribution.  
 331 We prove

332 **Theorem 2.** *Let  $T_1^{(n)}(x)$  and  $T_2^{(n)}(x)$  be the  $n$ th moments of the exit time conditioned on the*  
 333 *particle starting at position  $x$  with initial velocity  $+v$  and  $-v$  respectively. Then the moments*  
 334 *have the asymptotic behavior*

$$T_{1,2}^{(k)}(x) = \begin{cases} O\left(\frac{k!}{v^{2k}}\right), & v \ll 1, \\ O\left(\frac{k!}{v^k}\right), & v \gg 1. \end{cases} \quad (37)$$

335 *Proof.* We have  $T_{1,2}^{(n)}(x) = (-\partial/\partial s)^n \tilde{w}_{1,2}(x, s)|_{s=0}$  for  $n \geq 0$ , and from eqs. (9) and (10),  
 336 these moments satisfy the coupled equations

$$\begin{aligned} -v \frac{dT_1^{(n)}}{dx} - F(x)(T_2^{(n)} - T_1^{(n)}) &= nT_1^{(n-1)}, \\ v \frac{dT_2^{(n)}}{dx} - F(x)(T_1^{(n)} - T_2^{(n)}) &= nT_2^{(n-1)}, \end{aligned}$$

337 subject to the boundary conditions  $T_1^{(n)}(L/2) = 0$  and  $T_2^{(n)}(-L/2) = 0$  where  $n \geq 1$  and  
 338  $T_{1,2}^{(0)}(x) = 1$ . After some algebra, we find expressions for the moments in terms of indefinite  
 339 integrals:

$$T_1^{(n)}(x) = -\frac{n}{v^2} \int dx F(x) \int dx [T_1^{(n-1)}(x) + T_2^{(n-1)}(x)] - \frac{n}{v} \int dx T_1^{(n-1)}(x), \quad (38)$$

$$T_2^{(n)}(x) = -\frac{n}{v^2} \int dx F(x) \int dx [T_1^{(n-1)}(x) + T_2^{(n-1)}(x)] + \frac{n}{v} \int dx T_2^{(n-1)}(x). \quad (39)$$

340 When  $v \ll 1$ , we retain the first integral in each of eqs. (38) and (39) to find to obtain  
 341  $T_{1,2}^{(k)} = O(k!/v^{2k})$ . If  $v \gg 1$ , we retain the second integral to find  $T_{1,2}^{(k)} = O(k!/v^k)$ .  $\square$

342 In (37), we see that the moments have a different asymptotic form depending on whether  $v$   
 343 is small or large. When  $v \ll 1$ , the random walker is the diffusive limit where all the moments  
 344 (except for the zeroth moment) diverge. On the other hand, when  $v \gg 1$ , the particle is in  
 345 the ballistic limit: all moments except for the zeroth moment are asymptotically small and,  
 346 to leading order, independent of  $F(x)$ .

347 Now consider approximating  $w_1(x_0, t)$  or  $w_2(x_0, t)$  with their noisy counterparts generated  
 348 by the Monte-Carlo simulations. How well are the  $w_{1,2}(x_0, t)$  approximated? One way to  
 349 quantify the accuracy is by calculating the error in the moments of the noisy distribution.  
 350 Given an initial velocity  $+v$ , let  $\{\tau_j\}$ ,  $1 \leq j \leq N$  be the  $N$  generated exit times (the following

351 argument with initial velocity  $-v$  is almost identical). Then by the central limit theorem,  
 352 the  $k$ th moment is approximately distributed according to

$$\frac{1}{N} \sum_{j=1}^N \tau_j^k \sim \mathcal{N} \left( T_1^{(k)}, \frac{\text{Var}(\tau_j^k)}{N} \right),$$

353 where  $\mathcal{N}(\mu, \nu)$  is a normal distribution with mean  $\mu$  and variance  $\nu$ . Therefore a measure of  
 354 the error incurred when calculating the  $k$ th sample moment is

$$N^{-1/2} \sqrt{\text{Var}(\tau_j^k)} = N^{-1/2} \sqrt{T_1^{(2k)} - T_1^{(k)2}} = \begin{cases} O(N^{-1/2}v^{-2k}), & v \ll 1, \\ O(N^{-1/2}v^{-k}), & v \gg 1, \end{cases} \quad (40)$$

355 using (37) and  $\text{Var}(\tau_j^k) = E[(\tau_j^k - T_1^{(k)})^2]$ . Therefore from (40), a quick rule-of-thumb for  
 356 the accuracy of the Monte-Carlo generated exit time distribution is that the error scales as  
 357  $N^{-1/2}$  where  $N$  is the number of trials.

358 It is evident from (40) that for a fixed number of realizations, the error in the  $k$ th moment  
 359 diverges as  $v^{-2k}$  as  $v \rightarrow 0$  and the underlying exit time distribution is badly approximated  
 360 in the limit of small  $v$ . On the other hand, as  $v \rightarrow \infty$ , although the error in the moments  
 361 tend to zero, the moments themselves also tend to zero. From eq. (28) the probability that a  
 362 Broadwell particle with initial velocity  $+v$  exits in time  $t_c$  tends to 1 as  $v \rightarrow \infty$ : for large  $v$ ,  
 363 the generated list of exit times is populated almost exclusively by  $t_c$  (and  $t_c \rightarrow 0$  as  $v \rightarrow \infty$ ).  
 364 From a single exit time it is very difficult to infer any information about  $F(x)$ . In both  
 365 limiting cases, since the distribution of exit times is poorly captured by a finite number of  
 366 realizations, the quality of the reconstruction suffers.

367 Finally, we systematically explore the effect of noise on the reconstruction quality. In  
 368 Fig. 5, we plot the error of the reconstructed  $F_M(x)$  against the number of exits. For a wide  
 369 range of polynomials  $F^*(x)$ , using both the  $t$ - and  $s$ -methods, we find that the error in the  
 370 reconstructed function scales as  $O(N^{-1/2})$ . In particular, we see that for  $N = O(10^4)$ , the  
 371 error  $\|F_M - F^*\|_\infty = O(10^{-1})$  whereas  $N$  must exceed  $O(10^6)$  for the error to fall below  
 372  $O(10^{-2})$ . These estimates are mean values: the accuracy resulting from fitting one data set  
 373 to the next will always vary because the noise in each set is different.

## 374 4 Conclusions

375 In this paper, we made three contributions. The first is a pair of algorithms, Algorithms 4  
 376 and 5, that can be used to estimate the flip rate function of a 1D, constant-speed Broadwell  
 377 process from the distribution of exit times out of a finite interval. In particular, the  $t$ -method  
 378 is based on a novel series solution of the backward equation (5)-(8); see Theorem 1. The  
 379 second is a simulation method, Algorithm 3, that is used in this paper to generate the exit  
 380 times of a Broadwell particle. The algorithm can accommodate spatially dependent flip  
 381 rates and velocities. Our final contribution is a set of calculations and asymptotic results  
 382 that quantify the errors in approximating the exit time distribution with simulated data, and  
 383 the corresponding error in the flip rate reconstruction.

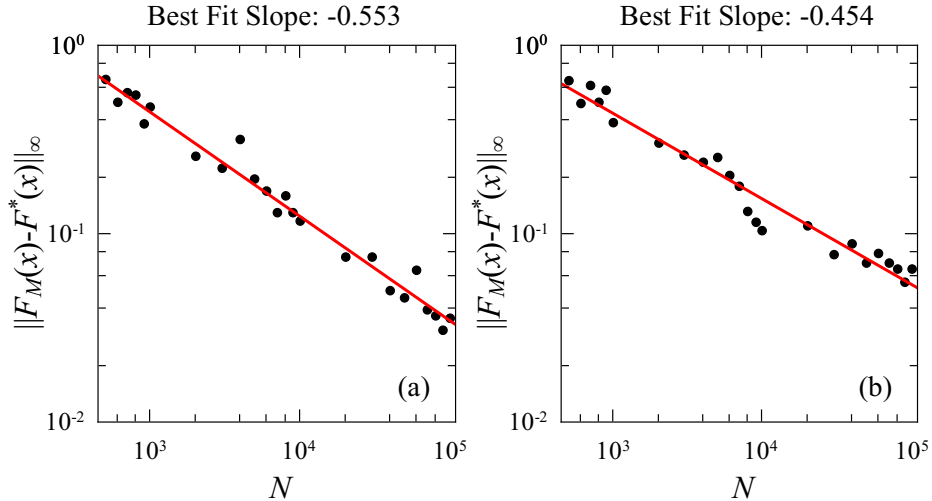


Figure 5: Dependence of error in reconstructed flip rate function  $F(x)$  on the number of exit times per initial particle state  $N$  when  $F(x) = 1 - 0.7x - 0.3x^2 + 6x^3$  using (a)  $t$ -method (b)  $s$ -method. For each  $N$ , the error is calculated by performing minimizations for 10 data sets and taking the average, with each set containing  $2N$  exit times.

384 We found that polynomial transition rates could be reconstructed if the degree of the  
 385 polynomial was not too large ( $\lesssim 4$ ) and that fitting to the exit time distribution ( $t$ -method)  
 386 directly versus fitting to the Laplace-transformed distribution ( $s$ -method) generally allowed  
 387 the reconstruction of one extra coefficient in the representation of  $F(x)$ . Providing our initial  
 388 guess for the coefficients of  $F(x)$  was not too far from the target coefficients, we were able  
 389 to find  $F(x)$  to within  $O(10^{-1})$  using  $O(10^4)$  exit times. We were also able to find good  
 390 approximations to non-polynomial flip-rate functions providing they are smooth and slowly  
 391 varying. Finally, we experimented with reconstructions using different advection speeds. We  
 392 found that  $v = O(1)$  yielded the most accurate reconstructions because very small or large  
 393 values of  $v$  in the Monte-Carlo simulations gave poor representations of the true underlying  
 394 exit time distribution.

395 Our results suggest that the  $t$ -method is an effective method to infer the spatially-  
 396 dependent flip rate function of a two-state Broadwell process, if it is known *a-priori* that this  
 397 function is smooth and structurally simple. The  $t$ -method involves explicitly solving for the  
 398 cumulative density functions (5)-(8), tracking the discontinuities via (12)-(13) and minimiz-  
 399 ing the objective function (33). With this method, one can often find  $M = 4$  coefficients from  
 400 about  $2N = 20,000$  exit times. The  $s$ -method usually reconstructs one less coefficient than  
 401 the  $t$ -method for the same number of exit times, and is more sensitive to the initial guess.  
 402 However, it is much simpler to implement and only involves solving the ordinary differential  
 403 equations (9)-(11) and minimizing (34).

404 We see two main extensions to this work. The first is to reconstruct spatially dependent  
 405 advection velocities  $v(x)$  as well as transition rates  $F(x)$ . The second is to develop alternative  
 406 algorithms for reconstruction. We showed in this paper that as the number of coefficients

407 representing the flip rate function increases, our method becomes unstable due to the presence  
 408 of flat minima in the objective functions (see eqs. (33) and (34) and Tables 1 and 2). This  
 409 instability could be alleviated by introducing a small regularization parameter in the objective  
 410 functions (33), (34) or developing iterative algorithms based directly on (1)-(3) and (5)-(8).

411 **Acknowledgements** PWF thanks Rakesh and Tobin Driscoll for helpful discussions. TC  
 412 was supported by the Army Research Office through grant 58386MA, and the National Sci-  
 413 ence Foundation through grant DMS-1021818. PWF and QH were supported by a University  
 414 of Delaware Research Foundation (UDRF) grant.

## 415 A Derivation of a multi-state Broadwell process

416 A one-dimensional generalized Broadwell model describes a particle that can take any one of  
 417  $K$  states. Initially, the particle is at position  $x$  and in state  $i$ . A particle in state  $1 \leq k \leq K$   
 418 advects within an interval  $(-L/2, L/2)$  with a velocity function  $v_k(y)$  that is single signed  
 419 on  $-L/2 \leq y \leq L/2$  with  $y$  being the current position. While advecting, the particle may  
 420 transition from state  $i$  to any other state  $j$  with probability  $F_{ji}(y)dt$  within time interval  
 421  $(t, t + dt)$ . Also  $F_{ji}(y)$  are positive functions when  $i \neq j$ , but  $F_{ii}(y) \equiv 0$ . The goal of this  
 422 appendix is to find the backward equation for the exit time distribution for such a process.

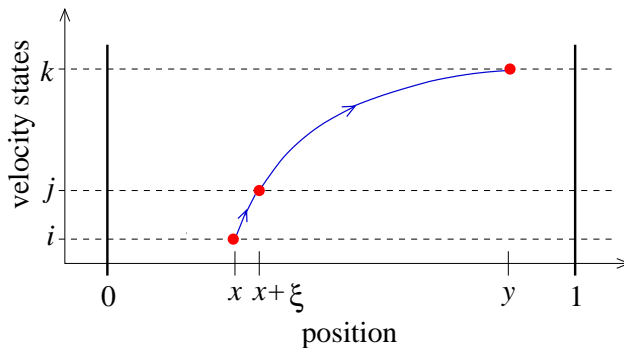


Figure 6: The transitions relevant for computing the Backward equation for the probability density of a multi-state persistent random walk. The quantities  $x$ ,  $x + \xi$  and  $y$  represent initial, intermediate and final positions while  $i$ ,  $j$  and  $k$  represent initial, intermediate and final states.

423 If  $P(y, k, t|x, i, 0)dy$  is the probability that the particle lies between  $y$  and  $y + dy$  and  
 424 is in state  $k$  at time  $t$ , given that it had started at position  $x$  in state  $i$  at time  $t = 0$ , the  
 425 Chapman-Kolmogorov equation [13] is

$$P(y, k, t + dt|x, i, 0) = \sum_{j=1}^K \int_{V_1 dt}^{V_2 dt} P(y, k, t + dt|x + \xi, j, dt)P(x + \xi, j, dt|x, i, 0)d\xi, \quad (41)$$

426 where  $V_1 = \min_k \min_{-L/2 < y < L/2} v_k(y)$ ,  $V_2 = \max_k \max_{-L/2 < y < L/2} v_k(y)$  and state  $k$  and posi-  
 427 tion  $y$  of the particle at time  $t + dt$  arise from accounting for all transitions from intermediate

428 states  $j$ ,  $j = 1, \dots, K$  and positions  $x + \xi$  at time  $dt$ : see Fig. 6. Note that  $V_1$  can be  
 429 negative and the integration over  $V_1 dt < \xi < V_2 dt$  corresponds to all possible displacements  
 430 from position  $x$ .

431 We will assume that the advection velocities and flip rates are explicitly time-independent  
 432 so that the process is time-homogeneous. Therefore, the probabilities are time-translationally  
 433 invariant and  $P(y, k, t + dt | x + \xi, j, dt) = P(y, k, t | x + \xi, j, 0)$ . In the following calculations,  
 434 we make frequent use of delta distributions so Taylor expansions and associated derivatives  
 435 are to be interpreted in the weak sense.

436 The probability of transition from  $(x, i)$  to  $(x + \xi, j)$  in time  $dt$  can be decomposed into  
 437 two terms corresponding to continued particle advection when no state flips occur in time  
 438  $dt$ , *or* a state change occurring within  $(0, dt)$ :

$$P(x + \xi, j, dt | x, i, 0) = \delta(\xi - v_i(x)dt) \left( 1 - \sum_{\substack{\ell=1 \\ \ell \neq i}}^K F_{\ell i}(x)dt \right) \delta_{ij} + \delta(\xi) F_{ji}(x)(1 - \delta_{ij})dt + O(dt^2). \quad (42)$$

439 The symbols  $\delta_{ij}$  and  $\delta(\cdot)$  are the usual Kronecker tensor and Dirac delta function, respec-  
 440 tively. The first term in Eq. 42 represents the probability that the particle did not transition  
 441 out of state  $i$  in  $(0, dt)$ , while the second term describes the transition probability from state  
 442  $i$  to state  $j \neq i$ .

443 In (42), when  $i = j$ , the term proportional to  $F_{ji}$  is zero (no state transitions have  
 444 occurred) and the probability density originally centered at  $x$  is simply advected to  $x + v_i(x)dt$ .  
 445 Therefore, the probability density of being in position  $x + \xi$  and state  $j = i$  at time  $dt$  is  
 446  $\delta(\xi - v_i(x)dt) (1 - \sum F_{\ell i}(x)dt)$ . When  $i \neq j$ , the term proportional to  $1 - \sum F_{\ell i}dt$  is zero. To  
 447  $O(dt)$ , we can ignore advection and simply assume the particle changed state in its current  
 448 position.<sup>1</sup> Therefore the probability of being at position  $x + \xi$  and state  $j$  at time  $dt$  is  
 449  $\delta(\xi) F_{ji}(x)dt$ .

450 Upon Taylor-expanding the remaining probability densities in (41):

$$P(y, k, t + dt | x, i, 0) = P(y, k, t | x, i, 0) + \frac{\partial P}{\partial t} dt + O(dt^2), \quad (43)$$

451

$$P(y, k, t | x + \xi, j, 0) = P(y, k, t | x, j, 0) + \frac{\partial P}{\partial x} \xi + O(\xi^2), \quad (44)$$

452 we find to order  $dt$  (note that  $\xi = O(dt)$ ),

$$\frac{\partial}{\partial t} P_{ki}(y, t | x, 0) = \sum_{j=1}^K L_{ji} P_{kj}(y, t | x, 0), \quad (45)$$

---

<sup>1</sup>If advection was included,  $\delta(\xi) F_{ji} dt$  in (42) would be replaced with  $\delta(\xi + O(dt)) F_{ji} dt$  corresponding to an additional displacement of  $O(dt)$  and an associated error of  $O(dt^2)$ .

453 where

$$P_{ki}(y, t|x, 0) \equiv P(y, k, t|x, i, 0), \quad L_{ji} = \delta_{ij}v_i(x)\partial_x + (1 - \delta_{ij})F_{ji} - \delta_{ij} \sum_{\substack{\ell=1 \\ \neq i}}^K F_{\ell i}. \quad (46)$$

454 When  $t \leq 0$ , the particle is at  $y = x$  in state  $i$  so that

$$P(y, k, t|x, i, 0) = \delta_{ik}\delta(x - y), \quad t \leq 0. \quad (47)$$

455 Henceforth, we consider the domain  $y \in (-L/2, L/2)$  with absorbing boundaries at  $y = \pm L/2$   
 456 so that when  $t > 0$  the appropriate boundary conditions are

$$\begin{aligned} P(y, k, t|x = +L/2, i, 0) &= 0, \quad \forall i : v_i > 0, \\ P(y, k, t|x = -L/2, i, 0) &= 0, \quad \forall i : v_i < 0. \end{aligned} \quad (48)$$

## 457 A.1 Survival Probabilities

458 If we do not distinguish from which boundary the particle eventually exits, we can define  
 459 the survival probability by integrating Eq. (45) over all positions  $y \in (-L/2, +L/2)$  and  
 460 summing over all possible final states. The survival probability

$$S_i(x, t) = \sum_{k=1}^K \int_{-L/2}^{L/2} P(y, k, t|x, i, 0) dy, \quad (49)$$

461 describes the probability that a particle started at position  $x \in (-L/2, +L/2)$  in state  $i$  has  
 462 not left through either boundary up to time  $t$ . When  $t \leq 0$ , we have from (47)

$$S_i(x, t) = 1, \quad -L/2 \leq x \leq L/2. \quad (50)$$

463 When  $t > 0$ , the survival probability obeys

$$\frac{\partial}{\partial t} S_i(x, t) = v_i(x) \frac{\partial}{\partial x} S_i(x, t) + \sum_{\substack{j=1 \\ \neq i}}^K F_{ji}(x) S_j(x, t) - \sum_{\substack{\ell=1 \\ \neq i}}^K F_{\ell i}(x) S_i(x, t), \quad (51)$$

464 with boundary conditions

$$\begin{aligned} S_i(L/2, t) &= 0, \quad \text{for } i : v_i(x) > 0, \\ S_i(-L/2, t) &= 0 \text{ for } i : v_i(x) < 0. \end{aligned} \quad (52)$$

## 465 A.2 Exit time distributions

466 The full exit time distribution is found from the usual definition  $w(t|x, i, 0) \equiv w_i(x, t) =$   
 467  $-\partial S_i(x, t)/\partial t$ , so differentiating Eq. (51), we have

$$\frac{\partial}{\partial t} w_i(x, t) = v_i(x) \frac{\partial}{\partial x} w_i(x, t) + \sum_{\substack{j=1 \\ \neq i}}^K F_{ji}(x) w_j(x, t) - \sum_{\substack{\ell=1 \\ \neq i}}^K F_{\ell i}(x) w_i(x, t). \quad (53)$$



468 The initial condition is found by differentiating (50) in time so that  $w_i(x, t) = 0$  when  $t \leq 0$ .  
469 In particular,

$$w_i(x, 0) = 0. \quad (54)$$

470 From (51) and (52), we have  $S_i(L/2, t) = S_i(-L/2, t) = H(-t)$  for all  $t$ . Therefore the  
471 boundary conditions for  $w_i(x, t)$  are

$$\begin{aligned} w_i(L/2, t) &= \delta(t), & \forall i : v_i > 0, \\ w_i(-L/2, t) &= \delta(t), & \forall i : v_i < 0. \end{aligned} \quad (55)$$

472 When  $K = 2$ ,  $F_{12}(x) = F_{21}(x) = F(x)$ ,  $v_1(x) = -v_2(x) = v$  (a positive constant), equations  
473 (53)-(55) reduce to (1)-(4).

## 474 References

- 475 [1] S. R. Arridge. Optical tomography in medical imaging. *Inverse Problems*, 41:41–93,  
476 1999.
- 477 [2] S R Arridge and J C Hebden. Optical imaging in medicine: II. Modelling and recon-  
478 struction. *Physics in medicine and biology*, 42(5):841–53, May 1997.
- 479 [3] S. Asmussen and P. W. Glynn. *Stochastic Simulation: Algorithms and Analysis*.  
480 Springer, 2010.
- 481 [4] Guillaume Bal and Tom Chou. On the reconstruction of diffusions from first-exit time  
482 distributions. *Inverse Problems*, 20:1053–1065, 2003.
- 483 [5] D. J. Bicout. Green’s functions and first passage time distributions for dynamic insta-  
484 bility of microtubules. *Physical Review E*, 56, 1997.
- 485 [6] J. E. Broadwell. Shock structure in a simple discrete velocity gas. *Phys. Fluids*, 7:1243,  
486 1964.
- 487 [7] J. E. Broadwell. Study of rarefied shear flow by the discrete velocity method. *J. Fluid*  
488 *Mech.*, 19:401, 1964.
- 489 [8] A. J. Christlieb, J. A. Rossmannith, and P. Smereka. The Broadwell model in a thin  
490 channel. *Comm. Math. Sci.*, 2:443–476, 2004.
- 491 [9] M. V. de Hoop, H. Smith, G. Uhlmann, and R. D. van der Hilst. Seismic imaging with  
492 the generalized radon transform: a curvelet transform perspective. *Inverse Problems*,  
493 25, 2009.
- 494 [10] Olga K Dudko. Single-molecule mechanics: New insights from the escape-over-a-barrier  
495 problem. *Proceedings of the National Academy of Sciences of the United States of Amer-*  
496 *ica*, 106(22):8795–6, June 2009.

- 497 [11] P.-W. Fok and T. Chou. Reconstruction of potential energy profiles from multiple  
498 rupture time distributions. *Proceedings of the Royal Society A: Mathematical, Physical*  
499 *and Engineering Sciences*, 466(2124):3479–3499, June 2010.
- 500 [12] L. B. Freund. Characterizing the resistance generated by a molecular bond as it is  
501 forcibly separated. *Proceedings of the National Academy of Sciences of the United States*  
502 *of America*, 106(22):8818–23, June 2009.
- 503 [13] C. W. Gardiner. *Handbook of stochastic methods*. Springer, 1985.
- 504 [14] M. T. Giraud and L. Sacerdote. An improved technique for the simulation of first  
505 passage times for diffusion processes. *Communications in Statistics - Simulation and*  
506 *Computation*, 28:1135–1163, 1999.
- 507 [15] M. T. Giraud, L. Sacerdote, and C. Zucca. A Monte Carlo method for the simulation  
508 of first passage times of diffusion processes. *Methodology and computing in applied*  
509 *probability*, 3:215–231, 2001.
- 510 [16] S. Goldstein. On diffusion by discontinuous movements and on the telegraph equation.  
511 *Quarterly journal of mechanics and applied mathematics*, 4:129–156, 1951.
- 512 [17] Gerhard Hummer and Attila Szabo. Kinetics from nonequilibrium single-molecule  
513 pulling experiments. *Biophysical Journal*, 85(1):5 – 15, 2003.
- 514 [18] R. Kress. *Linear Integral Equations*. Springer-Verlag, 1989.
- 515 [19] R. Mannella and V. Palleschi. Fast and precise algorithm for computer simulation of  
516 stochastic differential equations. *Physical Review A*, 40, 1989.
- 517 [20] J. Masoliver and G. H. Weiss. Telegrapher’s equations with variable propagation speeds.  
518 *Physical Review E*, 49:3852–3854, 1994.
- 519 [21] R. G. Novikov. The inverse scattering problem at fixed energy for the three-dimensional  
520 Schrödinger equation with an exponentially decreasing potential. *Communications in*  
521 *Mathematical Physics*, 161:569–595, 1994.
- 522 [22] C.-L. Guo P.-W. Fok and T. Chou. Charge-transport mediated recruitment of DNA  
523 repair enzymes. *Journal of Chemical Physics*, 129, 2008.
- 524 [23] P. Sacks and W. Symes. Recovery of the elastic parameters of a layered half-space.  
525 *Geophysical Journal of the Royal Astronomical Society*, 88:593–620, 1987.
- 526 [24] W. W. Symes. A differential semblance algorithm for the inverse problem of reflection  
527 seismology. *Computers and Mathematics with Applications*, 22:147–178, 1991.
- 528 [25] T. Taillefumier and M. O. Magnasco. A fast algorithm for the first-passage times of  
529 Gauss-Markov processes with Hölder continuous boundaries. *J. Stat. Phys.*, 140:1130–  
530 1156, 2010.
- 531 [26] L. N. Trefethen. *Spectral Methods in Matlab*. SIAM, 2000.